Evolution of Helium Platelets and Associated Dislocation Loops in α-SiC

J. Chen, P. Jung, and H. Trinkaus
Institut für Festkörperforschung, Forschungszentrum Jülich, D-52425 Jülich, Germany
(Received 5 October 1998)

Implantation of 2450 at. ppm helium into silicon carbide at room temperature results in the formation of helium platelets with surprisingly uniform diameters about 9 nm, remaining constant upon annealing up to 1270 K. Estimation of the pressure in the platelets suggests the presence of solid helium even above ambient temperature. The narrow size distribution and the limitation of growth of the platelets is attributed to their trapping by circular dislocation dipoles forming close to their rim when they reach a critical size. Upon annealing to $\approx$1500 K, the platelets disintegrate into disks of bubbles and, attached to them, interstitial-type dislocation loops appear. The total volumes of bubble and loop components in such complexes are found to be equal. This striking relation is attributed to the transfer of matrix atoms from the bubbles to the associated loops by dislocation core diffusion. [S0031-9007(99)08776-1]

PACS numbers: 61.82.Ms, 62.20.Mk, 61.72.Qq

Because of its extremely low solubility in crystalline materials, helium strongly tends to precipitate into bubbles [1,2]. At medium temperatures where He interstitial atoms are mobile but matrix atoms are still immobile, the absorption of He interstitial atoms by existing bubbles may result in the building up of extremely high pressures close to the theoretical shear strength of the material [3,4]. Thus, by implantation of mobile insoluble gas atoms into elastically very strong materials such as silicon carbides or even diamond, the highest static pressures in terrestrial laboratories may be attained [4]. It is of fundamental interest to study the conditions under which such pressures can be reached. From a practical point of view, helium bubbles in silicon carbide may be important for the proposed use of these materials in fusion reactors or in nuclear waste management as well as for the introduction of bubbles suggested for gettering metallic impurities in microelectronic devices.

Previous investigations on helium induced microstructural changes in SiC were confined either to shallow implantation of helium ions in the keV range [5] or to neutron irradiation of boron doped material [6,7]. In the present work, α particles with ranges up to $\approx$200 μm were used, allowing the study of helium clustering unaffected by surfaces (due to shallow implantation) or grain boundaries (due to boron segregation).

The material investigated was hot-pressed SiC of $\approx$98.5% purity and 3.2 g/cm^3 density (EKasic-HD). X-ray analysis and transmission electron microscopy (TEM) gave about 80% 6H-SiC, 18% 4H-SiC, and small amounts of 3C-SiC (β-SiC), 15R-SiC, and free carbon. Helium implantation was performed at room temperature with a 26.3 MeV α beam in a vacuum chamber ($\approx 10^{-3}$ Pa), using a degrader wheel to obtain homogeneous distribution up to maximum depths which could be adjusted up to 200 μm. Annealing was performed by dropping the specimens into a hot tube furnace in a UHV chamber. Estimated heating and cooling times were on the order of a few seconds. TEM foils were prepared by ion milling the specimens from both sides after annealing; for details, see Ref. [8].

Specimens irradiated at room temperature with transmitting protons, i.e., without helium implantation, to displacement doses up to 0.2 dpa (displacements per atom), showed no microstructural changes in TEM, neither after irradiation nor after subsequent annealing. This means that the amorphization dose for light ions is substantially higher than for Ar or Xe bombardment [9], and that all of the microstructural features observed after implantation of SiC are closely related to helium. After implantation of 2450 at. ppm helium ($2.26 \times 10^{22} \alpha$ m^{-2}, $\approx$0.15 dpa, for the calculation of the displacement dose see [10]) at ambient temperature, two-dimensional platelets in the grains became clearly visible by TEM (Fig. 1). These are similar but more pronounced than in Si [11], B_4C [12,13], Mo [14], Ti [15], and Ni [16]. The defects in the grain interior are separated by defect-free zones of about a 0.5 μm width from the boundaries. Analysis of the platelets in Fig. 1 gives habit planes of (0001) [Fig. 1(a)], and through-focal bright-field imaging clearly shows that the platelets are of a cavity type [Figs. 1(b) and 1(c)]. The size distribution of the platelets is surprisingly narrow with an average diameter of about 9 nm and an opening of $\approx$0.6 nm, corresponding to about 2.4 lattice distances along (0001). Upon annealing up to 1270 K, the number density of the platelets increases, but the diameter and opening of the platelets stay almost constant.

At lower concentrations, platelets become visible only after annealing to $\approx$1500 K. Also around this temperature, platelets start to transform into disks of spherical bubbles, and associated dislocation loops or even stacks of loops become visible (Fig. 2). These loops are of an interstitial type and have habit planes (0001) with Burgers vectors $\frac{1}{4}$ or $\frac{1}{6}$ of [0001] in 4H- and 6H-SiC, respectively. Only a few percent are on $(2\underline{1}\underline{1}0)$ or $(01\underline{1}0)$ habit planes. The vertical extension of stacks can be roughly estimated

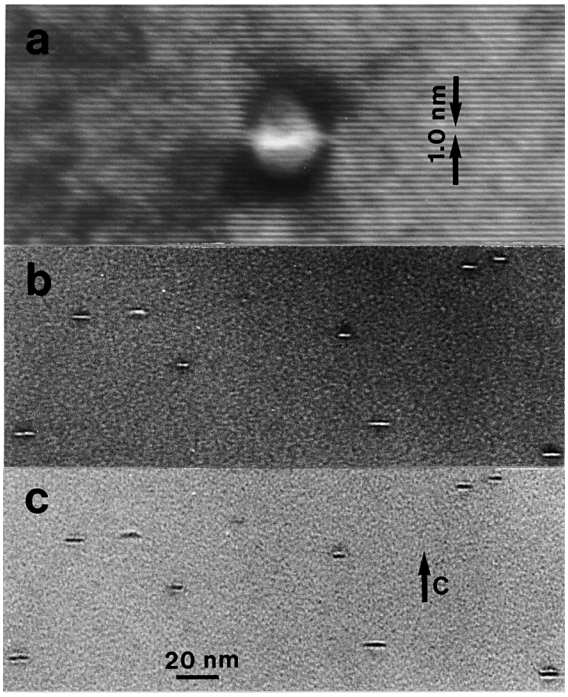

FIG. 1. Down-axis image with electron beam direction [2$\underline{1}\underline{1}$0] (a), and kinematic bright-field images [(b),(c)] with under-focused (b) and over-focused (c) beams of directions [01$\underline{1}$0], of a 4*H*-SiC grain as implanted with 2450 at. ppm He at ambient temperature. The stripes in (a) are superlattice fringes of 4*H*-SiC.

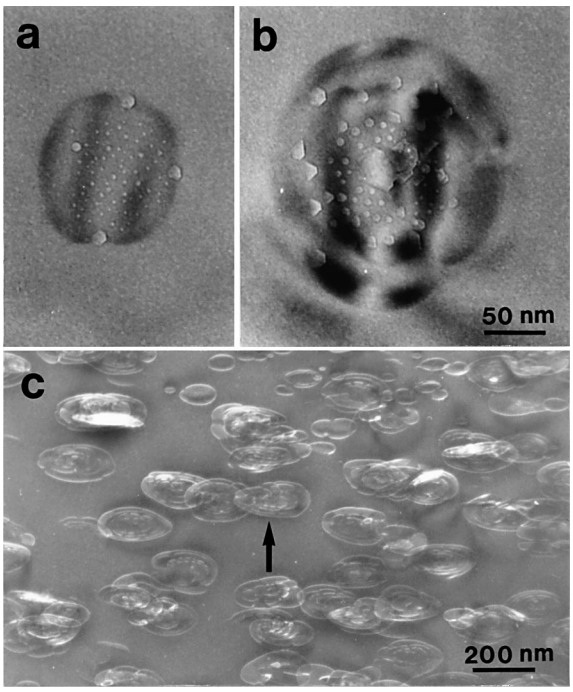

FIG. 2. Kinematic bright-field images of bubble-loop complexes [(a),(b)] and weak-beam dark field image (c) of loop stacks in 4*H*-SiC with 600 at. ppm He annealed at 1700 K for 1 h. Electron beam direction is close to [0001] in (a) and (b) and [03$\underline{3}$1] in (c). The arrow in (c) gives the g vector.

to ≈10 nm and their diameters to values closely around 220 nm, respectively. Apart from one observation near metallic precipitates in Si [17], this is the first time that stacks of interstitial-type loops are reported. Various types of bubble disks are observed, mostly with smaller bubbles in the middle and a few larger bubbles at the periphery, but also large central bubbles surrounded by smaller ones. A quantitative analysis of the bubble-loop complexes shows that the ratio of the total volume V_B of bubbles and the total area A_L of loops within a complex have an approximately constant value around 0.23 nm (Fig. 3). This ratio is in close agreement with the separation distance, 0.25 nm, of the (0001) planes. Above 1700 K the stacks of loops coalesce and form single loops. Annealing at ≥2100 K gives still larger loops that have lost the association with their bubbles. Also the average bubble size is increased but with a more homogeneous size distribution than at 1500 K, i.e., no large bubbles form.

In the following, these results will be rationalized in terms of diffusion and clustering of He and transformation of the resulting He platelets by matrix atom removal. In SiC the energetic α particles produce about 60 Frenkel pairs, mainly at the end of their range. During implantation ($T \leq 350$ K), interstitial helium atoms are sufficiently mobile to reach a vacancy thus forming substitutional helium [18]. A substitutional helium atom can become mobile again by the recombination of a self-interstitial atom (SIA) with the vacancy or by thermal dissociation. As the number of He atoms is still much lower than that of vacancies, formation of larger helium clusters during implantation of 2450 at. ppm cannot be due to remobilization of He by Frenkel pair recombination, but must be attributed to thermal dissociation from vacancies and long-range diffusion of interstitial helium. Thus, helium clusters should be able to grow continuously during implantation as well as during annealing by the absorption of newly implanted or resolved mobile He interstitials, respectively.

For the growth of He clusters by absorption of interstitial He, lattice space must be supplied. Possible mecha-

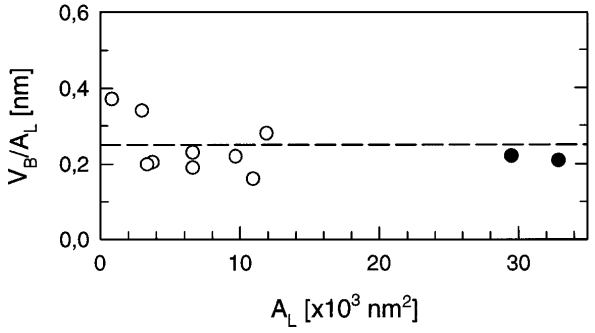

FIG. 3. Ratio of total volume of bubbles or bubble disks to the area of associated single (○) or multiple loops (●) of 4*H*-SiC with 600 at. ppm He after annealing for 1 h at 1700 K. The dashed line gives the separation of (0001) planes.

nisms for the removal of matrix atoms are (1) removal of atoms by thermal or irradiation induced vacancies (self-diffusion); (2) transport of matrix atoms along dislocation cores ("conservative climb"); (3) thermal or irradiation induced emission of SIAs and transport through the bulk; (4) emission and gliding away of dislocation loops due to repulsion by the overpressurized cluster ("loop punching") [19]. Diffusion measurements show that in SiC the first process takes off only above 2000 K [20,21]. The second process may become viable at temperatures $\geq$1400 K, if a similar relation to bulk diffusion as in metals is assumed. For metals, no experimental evidence exists for the third process, but only indications from desorption measurements ("trap mutation") [22,23], and from computer simulation [24,25]. On the other hand, loop punching has been observed by TEM in some metals (V, Mo). But in SiC probably neither SIAs (process 3) nor loops (process 4) can escape from the cluster, due to low mobility and high glide resistance, respectively. Under these conditions, the only way by which the cluster can acquire space is the formation of a crack, opened by a two-dimensional helium precipitate (platelet) between two lattice planes.

The pressure in such a platelet can be estimated by treating them as gas-filled, oblate ellipsoids of radius r and short axis s ($s \ll r$) [26], the free energy of which has elastic, surface, and gas contributions [27–29]. Oblate geometries are favored when elastic contributions dominate compared to surface energy [30]. Minimization with respect to r and s yields two equations from which expressions for pressure p and surface energy γ, corresponding to the Griffith criterion, can be derived:

$$p = \frac{\pi}{2} \frac{\mu}{(1-\nu)} \frac{s}{r}, \tag{1}$$

$$\gamma = \frac{\pi}{4} \frac{\mu}{(1-\nu)} \frac{s^2}{r} = p \frac{s}{2}, \tag{2}$$

where μ is the shear modulus and ν Poisson's ratio. With $\mu = 192$ GPa, $\nu = 0.16$, $r \approx 4.5$ nm, and $s \approx 0.3$ nm, Eqs. (1) and (2) yield $p \approx 24$ GPa and $\gamma \approx 3.6$ N/m^2, respectively. To our knowledge this value of γ represents the first, although crude, experimental determination of the (0001) surface energy of α-SiC. This value agrees reasonably with an estimate based on bond energies (3.1 eV) derived from the formation energy (1195 kJ/mol SiC), giving $\gamma \approx 3.5$ N/m, and also scales reasonably with γ of diamond. The high pressure value of 24 GPa gives a p/μ ratio close to the value of 0.2 as expected for loop punching [3] and has a very interesting consequence: By extrapolating the melting curve of helium, described by $p[\text{GPa}] \approx 1.691 \times 10^{-3} T_m^{1.555}$ for $0.1 \leq p \leq 2$ [31] to higher pressures, a melting point of $T_m \approx 468$ K is obtained. Thus helium in the platelets should clearly be solid at room temperature.

On the other hand, at such high pressures, the theoretical shear strength ($\mu/2\pi \approx 30$ GPa) may be exceeded at the rim of the crack and a circular edge dislocation dipole may form there (Fig. 4). It should be noted that this is not the conventional loop punching. The energy for the formation of the dipole is supplied by the relaxation of the pressure in the crack, i.e.,

$$E_{21} \leq \int_{p_0}^{p_1} p \, dV, \tag{3}$$

where p_0 and p_1 are the pressures before and after dipole formation. The critical crack size at which the formation of a dipole becomes favorable can be estimated by assuming a power law relation between pressure and volume at high pressures, i.e., $p/p_0 \approx (V_0/V)^\alpha$ with $\alpha = -(\partial \ln p/\partial \ln V)_T$. Using this in Eq. (3), we obtain

$$\frac{p_0 V_0}{\alpha - 1}[1 - (p_1/p_0)^{1-1/\alpha}] \geq E_{21}. \tag{4}$$

A value of $\alpha \approx 3$ can be estimated from an existing high pressure equation of state for helium [32]. If the formation energy of the dipole is estimated from the energy needed to create an internal surface ($E_{21} \approx 4\pi\gamma br$), Eqs. (2) and (4) give

$$\frac{r}{b} \leq \tfrac{3}{2}(\alpha - 1)/[1 - (p_1/p_0)^{1-1/\alpha}]. \tag{5}$$

The experimental values of $r \approx 4.5$ nm and $b = 0.25$ nm are consistent with Eq. (5) for a reasonable value p_1/p_0 of 0.76. Consequences of dipole formation are further helium absorption by the crack due to temporary pressure relaxation and inhibition of growth due to elastic constraints associated with the presence of the dislocation dipole. Pressure increase may induce the formation of a second dipole on the other side of the crack, but eventually helium absorption will cease when inflow and resolution become balanced. This explains the narrow size distribution of the cracks and its temperature independence up to 1270 K. Unfortunately, the postulated circular dislocation dipoles close to the rim of the cracks cannot be revealed by conventional TEM techniques, since the strain contrasts with and without such dipoles are expected to be rather similar. On the other hand, the high pressure platelets are stable only at specimen thicknesses which make high resolution TEM very difficult.

Around 1500 K, diffusion along the dislocation cores becomes fast enough to allow stress relaxation in the platelet by the transport of matrix atoms. The loops grow

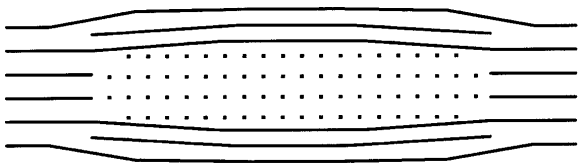

FIG. 4. Schematic view of the helium filled crack (platelet), constrained by two dislocation dipoles on both sides. The dots indicate solidified helium atoms.

by conservative climb, releasing the elastic constraint, and the partially relaxed cavities transform to the now more favorable spherical shape, i.e., the platelets are replaced by disks of bubbles. Also the kinetic constraint against Ostwald ripening by the exchange of helium atoms between bubble-loop complexes is released, resulting in an increase of their average size.

Transport of matrix atoms is fastest from the rim of the disk, which explains the larger bubble sizes there [Fig. 2(a)]. When at a certain size, diffusion to the rim of the dislocations becomes too slow, new loops are nucleated [Figs. 2(b) and 2(c)]. This explains the occurrence of stacks of loops with a narrow size distribution around 220 nm. Most probably loop nucleation takes place close to the center of the complexes, which favors the growth of large central bubbles in this case [Fig. 2(b)]. The much higher migration energy of atoms along the dislocations (about half self-diffusion energy) compared to helium diffusion explains why stacks are formed only in a narrow temperature range: With increasing temperatures the removal rate speeds up faster than helium absorption. So far, transport of matrix atoms is restricted within the complexes, explaining the observed exact equality of atomic sizes of cavities and associated loops (Fig. 3) [33]. Only around 2100 K this restriction is relieved, probably by the beginning of self-diffusion.

In future work, attempts should be made to prove the existence of dislocations loop dipoles close to the rim of gas-filled cracks, for instance, by high resolution electron microscopy. Furthermore, scanning tunneling microscopy (STM) could give more information on the arrangement of the stacks of loops. In addition, it should be tried to demonstrate that the helium enclosed in the cracks is crystalline at room temperature. We have started experiments with helium implanted diamond where the pressure is expected to be even higher than in SiC, and where it should be easier to obtain sufficient electron diffraction contrasts from the supposed helium crystallites within the platelets.

This work was performed under Association EURATOM-FzJ.

[1] R. S. Barnes and D. J. Mazey, Philos. Mag. **5**, 1247 (1960).
[2] H. Ullmaier, Nucl. Fusion **24**, 1039 (1984).
[3] W. G. Wolfer, Philos. Mag. A **58**, 285 (1988).
[4] H. Trinkaus, in *Fundamental Aspects of Inert Gases in Solids*, edited by S. E. Donelly and J. H. Evans, NATO ASI Ser. B, Vol. 279, p. 369.
[5] K. Hojou, S. Furuno, K. N. Kushita, H. Otsu, and K. Izui, J. Nucl. Mater. **191–194**, 583 (1992).
[6] J. C. Corelli, J. Hoole, J. Lazzaro, and C. W. Lee, J. Am. Ceram. Soc. **66**, 529 (1983).
[7] T. Suzuki, T. Yano, T. Mori, H. Miyazaki, and T. Iseki, Fusion Technol. **27**, 314 (1995).
[8] J. Chen, Ph.D. thesis, RWTH Aachen, Forschungszentrum Jülich [Report No. Jül 3585, ISSN 0944-2952, 1998].
[9] W. J. Weber, N. Yu, L. M. Wang, and N. J. Hess, J. Nucl. Mater. **244**, 258 (1997).
[10] Z. Zhu, Ph.D. thesis, Forschungszentrum Jülich [Report No. Jül-3109, ISSN 0944-2952, 1995].
[11] P. F. P. Fichtner, J. R. Kaschny, R. A. Yankov, A. Mücklich, and U. Kreißig, Appl. Phys. Lett. **70**, 732 (1997).
[12] A. Jostsons, C. K. H. DuBose, G. L. Copeland, and J. O. Stiegler, J. Nucl. Mater. **49**, 136 (1973).
[13] T. Stoto, J. Ardonceau, L. Zuppiroli, M. Castiglioni, and B. Weckermann, Radiat. Eff. **105**, 17 (1987).
[14] J. H. Evans, A. van Veen, and L. M. Caspers, Nature (London) **291**, 310 (1981).
[15] T. Schober and H. Trinkaus, Philos. Mag. A **65**, 1235 (1992).
[16] M. D'Olieslaeger, L. de Schepper, G. Knuyt, and L. M. Stals, J. Nucl. Mater. **138**, 27 (1986).
[17] O. Ueda, K. Nauka, J. lagowski, and H. C. Gatos, J. Appl. Phys. **60**, 622 (1986).
[18] P. Jung, J. Nucl. Mater. **191–194**, 377 (1992).
[19] M. I. Baskes, R. H. J. Fastenau, P. Penning, L. M. Caspers, and A. van Veen, J. Nucl. Mater. **102**, 235 (1981).
[20] J. D. Hong and R. F. Davis, J. Am. Ceram. Soc. **63**, 546 (1980).
[21] J. D. Hong, R. F. Davis, and D. E. Newbury, J. Mater. Sci. **16**, 2485 (1981).
[22] L. M. Caspers, R. H. J. Fastenau, A. van Veen, and W. F. W. M. van Heugten, Phys. Status Solidi (a) **46**, 541 (1978).
[23] J. H. Evans, A. van Veen, and L. M. Caspers, Radiat. Eff. **78**, 105 (1983).
[24] L. M. Caspers, M. Ypma, A. van Veen, and G. J. van der Kolk, Phys. Status Solidi (a) **63**, K183 (1981).
[25] W. D. Wilson, C. L. Bisson, and M. I. Baskes, Phys. Rev. B **24**, 5616 (1981).
[26] It should be noted that for small s/r ratios the measured value s^* of s strongly depends on the tilting angle β of the TEM specimen: $s^* \approx s + r \cdot \sin\beta$. For example, $\beta \approx 3.2°$ in Fig. 1 almost doubles s^* for the present ratio $s/r \approx 0.06$.
[27] I. N. Sneddon, Proc. R. Soc. London A **187**, 229 (1946).
[28] R. A. Sack, Proc. Phys. Soc. London **58**, 729 (1946).
[29] T. Mura, in *Micromechanics of Defects in Solids* (Nijhoff, The Hague, 1982).
[30] F. R. N. Nabarro, Proc. R. Soc. London A **175**, 519 (1940).
[31] R. L. Mills, D. H. Liebenberg, and J. C. Bronson, Phys. Rev. B **21**, 5137 (1980).
[32] H. Trinkaus, Radiat. Eff. **78**, 189 (1983).
[33] Such a quantitative analysis is not possible in metals as emitted atoms and/or punched loops readily move away.